*J. Fluid Mech.* (2004), *vol.* 502, *pp.* 89–98. © 2004 Cambridge University Press
DOI: 10.1017/S0022112003007729 Printed in the United Kingdom


# The wall-induced motion of a floating flexible train

By DOMINIC VELLA[1], HO-YOUNG KIM[2] AND L. MAHADEVAN[1]†

[1]Department of Applied Mathematics and Theoretical Physics, Cambridge University, Wilberforce Road, Cambridge, CB3 0WA, UK

[2]Thermal/Flow Control Research Center, Korea Institute of Science and Technology, Seoul 136-791, South Korea

(Received 26 September 2003 and in revised form 5 December 2003)

We consider the dynamics of capillary attraction between an articulated train of rigid rods floating at a liquid–gas interface and a nearby wall. We then explain some of the phenomena that are a result of the strong anisotropy and the extended nature of the system, such as the lining up next to the walling in a 'zippering' motion that is observed and compare our results qualitatively with those of experiments.

## 1. Introduction

Objects floating at the interface between two liquids distort the interface because of the vertical force balance between the interfacial tension ($\gamma$) tending to keep them at the interface and another force (such as gravity) that tends to pull the object into one fluid rather than the other. These interfacial distortions affect other objects at the interface and result in a mutual attraction or repulsion. The static configurations that result from such attractive interactions have been extensively studied, and the 'auto-tessellation' that often results may have technological applications (see Whitesides & Grzybowski 2002). Indeed, this type of system where there is a long-range attraction and a short-range (steric) repulsion was used more than fifty years ago by L. Bragg and his colleagues (Bragg & Nye 1947) to construct macroscopic models of crystalline solids using bubble rafts. However, the dynamics of these interactions are still incompletely understood, and have been the focus of recent investigations (Vincze *et al.* 2002). Furthermore, the primary emphasis of nearly all previous work has been on the interaction of rigid, near-isotropic isolated objects such as small spheres or polygonal plates.

Here, we consider the motion of highly anisotropic objects such as long slender needles floating at the air–water interface. Our motivation is to study the effects of the geometrically induced anisotropy and connectivity (topology) in these problems. The anisotropy induces orientational effects, while the connectivity introduces constraints that lead to interesting dynamical effects. We start by considering the case of a single cylindrical rod floating near an attractive wall, which is sufficient for understanding the interaction between two floating needles (observed by Gifford & Scriven 1971) because of the obvious symmetry. We then construct a train of needles by attaching them end-to-end with perfectly flexible hinges and study the dynamics of such a

† Present address: Division of Engineering and Applied Sciences, Harvard University, Cambridge, MA 02138, USA.

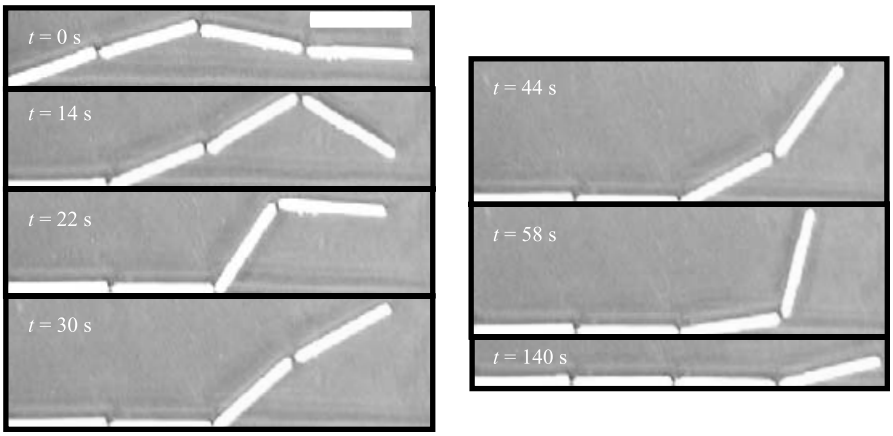


FIGURE 1. Snap-shots of the complex 'zippering up' motion for four connected candles at an air–water interface near a wall (at the bottom edge of each frame, just out of shot). The relevant Bond number here is $B \sim 0.5$ and the scale bar represents 4 cm.

structure when it is close to a wall. An example of this is shown in figure 1 where four beeswax candles connected by a thin polymer thread float at an interface between air and a syrup/water mixture in the neighbourhood of a vertical wall. Due to the attractive interfacial forces between the train of candles and the wall, the flexible train lines up next to the wall in a 'zippering' motion as a front propagates along it.

While here we will focus only on the simplest possible dynamical problems, the methods we use may be applied to understanding more generally the motion of flexible objects at an interface, and allow the construction of two-dimensional macroscopic analogues of packing processes such as the folding of DNA or proteins, with the spontaneous packing being a result of surface tension.

## 2. The capillary interaction between a horizontal rod and a wall

To understand the capillary interaction between a floating cylindrical rod and a fixed wall (as depicted in figure 2), we will use a simplified theory developed by Nicolson (1949), which is based on the following physical argument. For small Bond numbers, i.e. when the floating object's radius is less than the capillary length so that capillary forces dominate gravitational forces, the cylinder has gravitational potential energy because it lies at the top of a local hill (the interface) that is not significantly changed by its presence. Later work (Gifford & Scriven 1971) used detailed numerical simulations of the associated free boundary problem to find the attractive force, although the form of these results in the small Bond number limit was only explained in terms of the Nicolson approximation subsequently (Chan, Henry & White 1981).

Small deformations of the liquid–gas interface $\zeta(x, y)$ when just the wall is present satisfy the equation

$$\nabla^2 \zeta = \frac{\zeta}{L_c^2} \tag{2.1}$$

where $L_c = \sqrt{\gamma/\rho g}$ is the *capillary length*. In the two-dimensional geometry relevant here, (2.1) must be solved with the boundary conditions

$$\zeta_y(0) = -\cot\theta_1, \qquad \zeta(\infty) = 0, \tag{2.2}$$

so that $\zeta(y) = \cot\theta_1 L_c \exp(-y/L_c)$ where $\theta_1$ is the three-phase contact angle for the

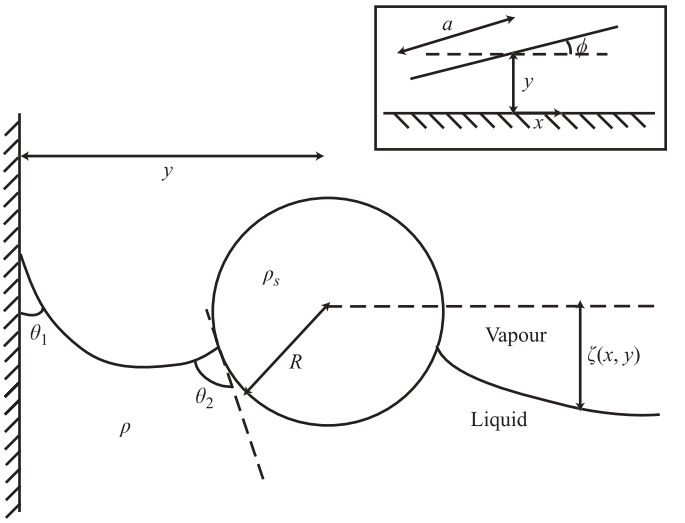


FIGURE 2. The geometry of a single rod floating near a wall: cross-section showing the physical parameters of the problem. Inset: a plan view showing the centreline of the rod and the wall.

liquid in contact with the plane (see figure 2). For a cylinder placed at the already deformed interface, with its axis parallel to the wall and its centre a horizontal distance $y$ from it, the Nicolson approximation yields the energy of attraction per unit length as

$$V(y) = \gamma L_c \cot\theta_1 BC \exp\left(-\frac{y}{L_c}\right). \tag{2.3}$$

This may be interpreted as the deformation of the interface $\zeta(y)$ multiplied by a constant whose value depends on the geometry of the floating object and is given for the cases of a cylinder and a sphere by Chan *et at.* (1981). Here, $B = \rho g R^2/\gamma$ is the *Bond number* and $C = \pi(D-1) + \theta_2 - \sin(2\theta_2)/2$ is a dimensionless constant, which, when multiplied by $\cot\theta_1$, determines whether the capillary force is attractive or repulsive. (It is thus possible to tune this interaction from being attractive to repulsive, without changing any of the surface chemistry, simply by altering the density of the cylinder. This is caused by a change in the interfacial shape which in turn is due to the change in the vertical force balance (between capillarity and gravity). This possibility appears not to have received much attention in the literature and is only hinted at by Paunov *et al.* 1993.) When the rod is inclined at an angle $\phi$ to the vertical plane (see the inset of figure 2 for the geometry) and the rod's centre is a distance $y$ from the plane, then the potential energy is modified to

$$V(y) = k\mathrm{e}^{-y/L_c}\frac{\sinh((a/L_c)\sin\phi)}{\sin\phi} \tag{2.4}$$

where $k = 2\gamma L_c^2 \cot\theta_1 BC$.

## 3. Dynamics of a single rod attracted to a wall

We shall use an energy formulation of the problem from the outset writing the Lagrangian, $\mathfrak{L}$, of the system as

$$\mathfrak{L} = \tfrac{1}{2}m(\dot{x}^2 + \dot{y}^2) + \tfrac{1}{2}I\dot{\phi}^2 - k\mathrm{e}^{-y/L_c}\frac{\sinh((a/L_c)\sin\phi)}{\sin\phi}. \tag{3.1}$$

Here the first two terms correspond to the translational and rotational kinetic energy of the rod, while the last term reflects the potential energy of (2.4), with $m$ the mass of the rod, $I$ its moment of inertia and $x$ and $y$ the coordinates of the centre of the rod. The orientation of the rod is denoted by $\phi$ (see figure 2). We model the hydrodynamic effects by assuming that the motion occurs at low Reynolds number and hence include the appropriate Stokes drag terms. Such an assumption is reasonable since a typical Reynolds number (based on a rod radius $R = 1$ mm, a velocity of 1 mm s$^{-1}$ and a kinematic viscosity $\nu = 10^{-4}$ m$^2$ s$^{-1}$) is $Re = 0.01$. These viscous effects are most conveniently included in our treatment by using a Rayleigh dissipation function, $\mathfrak{R}$ (Rayleigh 1945):

$$\mathfrak{R} = \tfrac{1}{2}\sigma_{\parallel}(\dot{x}^2\cos^2\phi + \dot{y}^2\sin^2\phi) + \tfrac{1}{2}\sigma_{\perp}(\dot{x}^2\sin^2\phi + \dot{y}^2\cos^2\phi) + \tfrac{1}{2}\sigma_{\circ}\dot{\phi}^2 - (\sigma_{\perp} - \sigma_{\parallel})\dot{x}\dot{y}\sin\phi\cos\phi \quad (3.2)$$

where $\sigma_{\perp}$ and $\sigma_{\parallel}$ are the rod's drag coefficients perpendicular and parallel to its axis and $\sigma_{\circ}$ is the drag coefficient associated with rotation about an axis perpendicular to the interface. The last term in the dissipation function couples the translational degrees of freedom to the rotational degrees of freedom only in the presence of an anisotropic drag, and arises purely on the grounds of symmetry (see, for example Happel & Brenner 1965). However, we have assumed, for simplicity, that the hydrodynamic effects of the wall and, when we consider trains of connected rods, the other rods are sufficiently small to be ignored. In a more careful analysis the dependence of the drag coefficients $\sigma$ on these other effects would have to be included although this will enter via a weak logarithmic factor. The Rayleigh dissipation function accounts for the drag on the rod and modifies the Euler–Lagrange equations to

$$\frac{\mathrm{d}}{\mathrm{d}t}\left(\frac{\partial\mathfrak{L}}{\partial\dot{q}}\right) - \frac{\partial\mathfrak{L}}{\partial q} + \frac{\partial\mathfrak{R}}{\partial\dot{q}} = 0 \quad (3.3)$$

where $q$ is a generalized coordinate. The equations of motion are then

$$m\ddot{x} = -\dot{x}(\sigma_{\parallel}\cos^2\phi + \sigma_{\perp}\sin^2\phi) + \dot{y}(\sigma_{\perp} - \sigma_{\parallel})\sin\phi\cos\phi,$$
$$m\ddot{y} = -\frac{k}{L_c}\mathrm{e}^{-y/L_c}\frac{\sinh((a/L_c)\sin\phi)}{\sin\phi} + \dot{x}(\sigma_{\perp} - \sigma_{\parallel})\sin\phi\cos\phi - \dot{y}(\sigma_{\parallel}\sin^2\phi + \sigma_{\perp}\cos^2\phi),$$
$$I\ddot{\phi} = k\cot\phi\mathrm{e}^{-y/L_c}\left((a/L_c)\cosh((a/L_c)\sin\phi) - \frac{\sinh((a/L_c)\sin\phi)}{\sin\phi}\right) - \sigma_{\circ}\dot{\phi}, \quad (3.4)$$

These equations of motion are solved numerically (using the adaptive step routine in *Mathematica*) once a short-range repulsive force is used to prevent the rod from moving through the wall. For simplicity, we adopt an exponential repulsion of the form $A_1\exp(-A_2(y - R))$ where $A_{1,2}$ are arbitrary parameters with the proviso that $A_2 \gg 1$ to ensure that the effect of the repulsive force is confined to a boundary layer near the wall. Assuming this form for the force law means that the equations of motion are altered by a term very similar to the capillary interaction, but using a more conventional Lennard–Jones potential does not alter the results.

We pause to consider a possible inconsistency since we have assumed a Stokes drag law but have at the same time included the inertia of the particle. This is not a problem if the ratio of the fluid inertia to the particle inertia, $\alpha$,

$$\alpha = \frac{\rho U^2}{\rho_s U^2} = \frac{\rho}{\rho_s}, \quad (3.5)$$

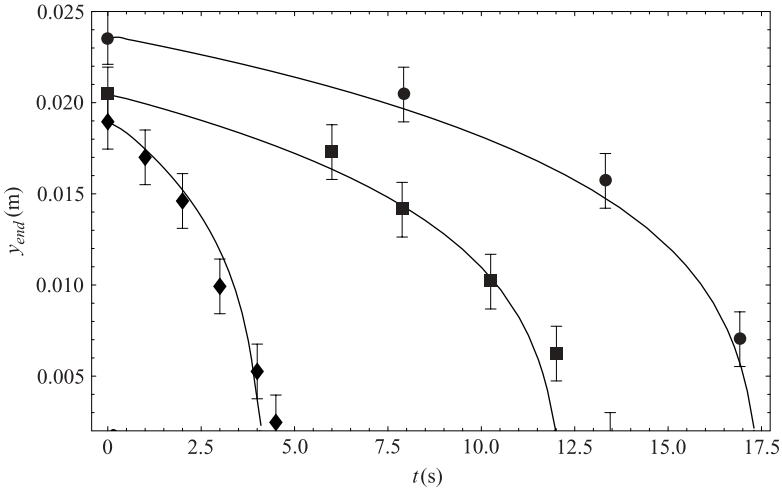


FIGURE 3. Experimental results and simulations for the case of a single rod as it zips up against a wall. Experiments were performed with two different water–glycerol mixtures: $\rho = 1180\ \mathrm{kg\,m^{-3}}$, $\gamma = 0.0652\ \mathrm{N\,m^{-1}}$, $\mu = 0.0225\ \mathrm{Pa\,s}$, $B = 0.40$, $\theta_1 = 95°$ and $\theta_2 = 86°$ corresponding to the data ● and ■; and $\rho = 1110\ \mathrm{kg\,m^{-3}}$, $\gamma = 0.047\ \mathrm{N\,m^{-1}}$, $\mu = 0.0158\ \mathrm{Pa\,s}$, $B = 0.52$, $\theta_1 = 35°$ and $\theta_2 = 99.5°$, corresponding to the data ◆.

is small. In many of the practical situations in which self-assembly occurs, the floating objects have a density much larger than that of the surrounding fluid (typically a metal component floating on water), so that $\alpha \sim 0.1$. In these situations, our approach is valid and we may consistently include the particle inertia but ignore the fluid inertia because of the large density differences. In other situations, when the ratio $\rho/\rho_s \sim O(1)$, the inclusion of inertia simply gives rise to an initial layer at small time, $t \leqslant t_{in} \sim m/\sigma_\perp$, during which inertia is important; over longer times viscous effects dominate. With the parameters typical for the experiments considered here (and shown in figure 1) we have $t_{in} \sim 0.1$ s so that the effects of inertia are short lived provided that the mass of the rods is small.

To determine the drag coefficients of a rod at the interface and hence calibrate the theory, we carried out experiments with two different liquids by floating small lengths of thermo-shrink tubing ($a = 0.015$ m, $R = 0.0015$ m and $\rho_s = 463$ kg m$^{-3}$) at the liquid–vapour interface near a fixed wall. These rods were placed with one end in contact with the wall so that we observed just the relatively slow zipping motion. The experimental results showing the distance of the free end of the rod from the wall, $y_{end}$, as a function of time are presented in figure 3 along with the results obtained by solving the equations of motion (3.4) numerically with an effective drag of the rod at the interface (since it is not completely immersed in either phase). The value of this effective drag coefficient is in the range [0.4, 0.45] times the drag of the same rod when completely immersed in the liquid. This value of an effective drag seems to accord with our intuition: since the rod floats a little less than half-immersed in the bulk it should have roughly half the associated drag.

## 4. Train dynamics

Having thus calibrated our model, we now study the case of many rods connected by a hinge that has no resistance to bending but is of a fixed length (together

constituting a flexible, inextensible train). We shall consider the dynamic capillary interaction between a wall and the train by neglecting the capillary interaction between the constituent rods and assuming instead that the effect of the wall is dominant. That this is the case in most experiments can easily be seen since the train will zipper-up against the wall rather than spontaneously fold in on itself, but is also explained by the analytical work of Chan *et al.* (1981): the capillary interaction between two horizontal cylinders at an interface scales like the product of the radii squared and so is insignificant compared to the wall–cylinder interaction given by (2.3) which scales like the radius squared. The dynamics of a train is interesting primarily because of the non-capillary interactions that arise as a result of the inextensible connection between the rods.

To facilitate the inclusion of this constraint, we adapt the Lagrangian used in the last section by adding terms of the form (3.1) together, where the positions and orientations of the rods are given by $(x_i, y_i, \phi_i)$ $(i = 1, \ldots, n)$. The constraints are accounted for using the technique of Lagrange multipliers, subject to the condition that the Lagrangian varies in a direction orthogonal to the gradient of the constraints. The integration of the equations of motion that result is only complicated by the presence of unknown Lagrange multipliers appearing in them. To deal with this, we adopt an approach similar to that used in the investigation of the dynamics of coupled pendulums by Ruhoff, Præstgaard & Perram (1996).

The constraints can be written in the form $\boldsymbol{f}(\boldsymbol{q}) = 0$, where $\boldsymbol{q}$ is the vector describing the positions and orientations of the rods. In particular, $\boldsymbol{f}$ is given by

$$f_{2i-1}(\boldsymbol{q}) = 0 = q_{3i+1} - q_{3i-2} - a(\cos q_{3i} + \cos q_{3i+3}), \tag{4.1}$$

$$f_{2i}(\boldsymbol{q}) = 0 = q_{3i+2} - q_{3i-1} - a(\sin q_{3i} + \sin q_{3i+3}), \tag{4.2}$$

for $i = 1, \ldots, n$. (Because we have adopted coordinates $(x_i, y_i, \phi_i)$ for each rod the constraints take the slightly long-winded form given here. The use of these coordinates makes other calculations simpler and so is adopted throughout). In general, we may write the equations of motion as

$$\ddot{\boldsymbol{q}} = \boldsymbol{M}^{-1}(\nabla_{\boldsymbol{q}} V - \boldsymbol{J}\boldsymbol{\lambda} - \boldsymbol{F}_D) \tag{4.3}$$

where $\boldsymbol{M}$ is the diagonal matrix whose elements consist of the mass of the rod and its moment of inertia, $\boldsymbol{J}$ is the Jacobian matrix of the constraints $J_{i\alpha} = \partial f_\alpha / \partial q_i$, $\boldsymbol{\lambda}$ is the vector of Lagrange multipliers and the added term $\boldsymbol{F}_D$ is the Stokes drag term given by the added Rayleigh dissipation term. By the chain rule we also have that

$$0 = \frac{\mathrm{d}^2 f_\alpha}{\mathrm{d}t^2} = \sum_{j=1}^{3n} J_{j\alpha}\ddot{q}_j + \sum_{i=1}^{3n}\sum_{j=1}^{3n} \dot{q}_i \frac{\partial J_{i\alpha}}{\partial q_j}\dot{q}_j. \tag{4.4}$$

Substituting into this the expression for $\ddot{\boldsymbol{q}}$ from (4.3) yields an expression for the unknown Lagrange multipliers $\boldsymbol{\lambda}$. After substituting these values back into (4.3) the numerical integration of the equation of motion is now relatively simple, although at each time step we must project the solution back onto the constraint surface. This is done using the constraint correction scheme of Ruhoff *et al.* (1996).

## 5. Numerical results

The space of possible initial train configurations is immense, so the results presented here are by no means exhaustive but merely exhibit some of the interesting dynamic phenomena that are observed. In fact, we shall only address three obvious questions

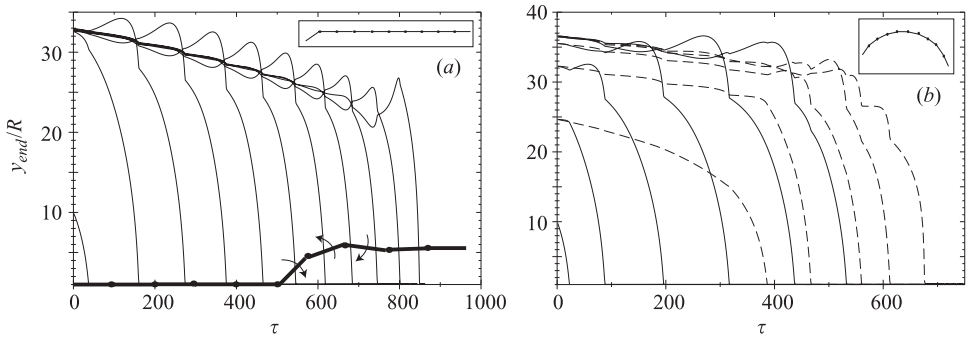


FIGURE 4. For a train consisting of ten rods, the end-of-rod distance is shown as a function of time. Insets: schematic of the initial configuration of the rods with circular dots representing the hinges. In (*a*) the propagation of the inversion wave is evident. The thick black line overlaying the lower portion of this graph is a schematic representation of the train seen from above at $\tau = 500$ with arrows showing the directions of rotation for the rods most involved in flicking. In (*b*) we see that rods on the shorter segment of the train (dashed line) zip up against the wall much later than the corresponding rods on the longer segment (solid line). The parameters in these graphs are: $\alpha = 0.1$, $B = 0.049$, $Re \sim 10^{-2}$, $a/R = 20$, $\theta_1 = 1.3$ rad and $\theta_2 = 1.4$ rad.

that might be asked about the dynamics of a single train: (*a*) What is the nature of the zipping motion for this extended system? (*b*) Does a train that, when viewed from above, initially resembles a monotonic function of the distance along the wall remain monotonic for all time? (*c*) Do those ends of the train that start closest to the wall always hit the wall first? We shall see that the answer to the first leads to an interesting question of front propagation, while the answer to the last two questions is in the negative even for relatively simple initial conditions.

Our numerical experiments use a variety of different initial configurations (although we always started the rods from rest). Initially we studied long trains with several hundred constituent rods but found that the results obtained are qualitatively very similar to those obtained with trains of up to ten rods.

The numerical results are presented in dimensionless terms with lengths being scaled by the radius of the rod $R$ rather than the capillary length $L_c$ and times being scaled by $R/v_{typ}$, where

$$v_{typ} = \frac{\gamma L_c \cot\theta_1 BC}{4\pi\mu a}\left(\ln\frac{2a}{R} - 0.5\right); \tag{5.1}$$

$v_{typ}$ is a characteristic velocity obtained from a naive balance between the perpendicular Stokes drag on the rod and the capillary force (scaled as the potential $V$ divided by the capillary length, $L_c$).

### 5.1. *Non-monotonicity*

Starting with a train at rest where all but one of the rods are parallel and one of the end rods is at an angle to the wall (see the inset of figure 4*a*), we see immediately that monotonicity is not preserved. Plotting the distance of the end points of each rod from the wall, as in figure 4(*a*), we see that successive rods have one end flicked out as their predecessor is attracted to the wall but that the other end stays roughly where it was. This monotonicity breaking is propagated along the train in a discrete 'inversion' wave.

The explanation for this effect is simple and is shown pictorially in the schematic configuration of the rod superimposed on the numerical results in figure 4(*a*). When one rod is in the final rotating motion towards the wall (i.e. one of its ends has already touched the wall), the rod connected to it is flicked out because of the torque associated with the tension that keeps this rod in contact with the rotating rod. This flicking of the second rod in turn affects the third rod since one of its ends is also flicked, although the effect is smaller at this point since the tension acting at the hinges is smaller. This explanation suggests that reducing the viscosity of the medium will reduce this effect, while increasing it will enhance the effect, as is observed numerically.

We expect from this explanation for the flicking motion that the initial distance of the rods from the wall is of crucial importance in determining the form of the wave and even whether it propagates at all. Indeed, we should expect that if the horizontal portion of the initial shape is closer to the wall then the size of the flick will decrease as there is not so much necessity for the first rod to rotate as it zips up. This is indeed observed and by decreasing the distance of the horizontal portion from the wall sufficiently, we can cause the wave to disappear at arbitrary points along the train.

The discrete wave observed in these numerical results has a wave speed associated with it dependent on the various parameters of the system. Although such a concept is ill defined because of the discreteness, there remains the characteristic velocity $v_{typ}$ used in the non-dimensionalization of time, and so we conclude that $v_{wave} \approx v_{typ}$. The precise value of the wave velocity will be dependent upon the exact form of the initial conditions but the above estimate is indeed a good one (to within a factor of 2) for a range of values of the parameters. The dependence on the initial configuration arises because of the dependence of the drag force on the orientation of the rods. The fact that this wave is reproduced in simulations where the density ratio $\alpha \sim O(1)$ (and hence inertia is negligible in all but a very short initial layer) is also confirmation that the front is a result of the geometry of the situation, the attractive force and the viscosity of the liquid, rather than particle inertia.

### 5.2. *Non-preservation of order*

To illustrate that the rods do not necessarily touch the wall in the order we might expect, we start with the train in a parabolic shape, consisting of two unequal segments joined by a horizontal rod. The shorter segment consists of four rods while the longer segment consists of five and so has one rod closer to the wall initially than the shorter segment (see the inset of figure 4*b*). In figure 4(*b*) we see that the rods on the longer segment touch the wall before some of their counterparts on the other segment even though they were initially further away. This is clearly a manifestation of the inextensibility constraint: the tip of the longer segment touches the wall first and then pulls the rest of that segment with it helping them to beat their counterparts on the shorter segment.

## 6. Experimental results

Having seen the behaviour predicted by the simple model presented above, we now turn to the original experiments that motivated this study. Returning to figure 1, we see that there is qualitative agreement between the observed phenomena and the model results. In particular, we see snapshots of the propagation of the inversion wave and also that the rightmost rod, despite starting close to the wall, zips up last.

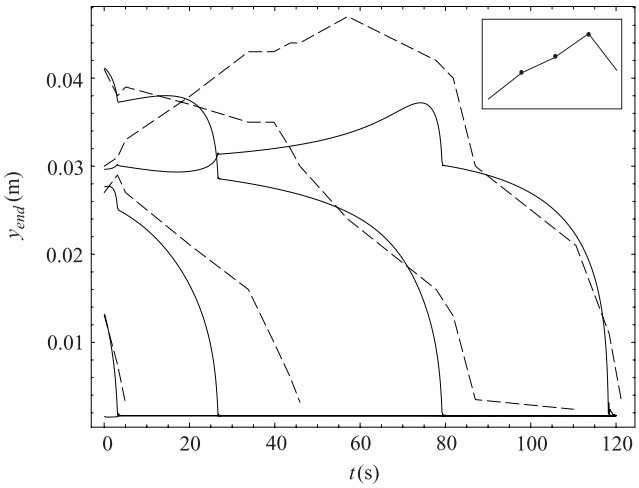


FIGURE 5. The distance–time graph of the ends for a train consisting of four rods. The theoretical results (solid lines) are compared with experimental values (dashed lines). The parameter values used in the model were $\theta_1 = 99°$, $\theta_2 = 80°$, $B = 0.4$ and $\alpha = 2.55$. Inset: schematic of the initial configuration of the rods with circular dots representing the hinges.

To check some of the predictions of the model, trains consisting of around five rods were fabricated (initially the trains contained up to ten rods but these quickly disintegrated owing to the delicate strand of polymer connecting them). The rods were cut from small sections of thermoshrink tubing and connected by a thin (diameter $\sim 10\,\mu$m) very short polymer thread, which acted as a flexible hinge. The trains were floated at the interface between a 2:1 glycerol/water solution and air (so that $\gamma = 0.0652\,\mathrm{N\,m^{-1}}$ and $\mu = 0.0225$ Pa s; the effective drag coefficients on the partly immersed cylinder are assumed to be 0.4 times the drag coefficients when the cylinder is completely immersed).

The fabricated train (finally consisting of four rods) was floated with one end in contact with the wall. The experimental results are shown in figure 5 and compared to the predictions of the model there. Although the comparison is not particularly favourable quantitatively, we see that the qualitative trends are similar to those predicted by our model. The main difference between theory and experiment is that the evolution of the zipping is delayed somewhat in reality, which is most likely a manifestation of the way the rods are connected to each other. For example, the polymer thread which connects the rods is almost certainly is not the perfect hinge assumed in the model; it has a finite length and a small but finite bending stiffness.

## 7. Discussion

In obtaining the equations of motion (3.4), we made a number of assumptions whose validity we shall consider briefly. A typical Reynolds number here is $Re = 0.01$ (based on a rod radius $R = 1$ mm, a velocity of 1 mm s$^{-1}$ and a kinematic viscosity $\nu = 10^{-4}$ m$^2$ s$^{-1}$, which is 100 times that of water) and so the assumption of low Reynolds number is reasonable. We also assumed that the drag of rods at an interface is of the same form as the drag of the rod within the bulk fluid but with a lower effective viscosity. To remove this assumption an analysis similar to that of Danov, Dimova & Pouligny (2000) for a rod at an interface would be required. We also used the

Nicolson approximation to calculate the interaction between the cylinder and the wall. In a more refined analysis an approach similar to that of Gifford & Scriven (1971) could be used to calculate the interaction force numerically which would liberate our analysis from the restriction that $B \ll 1$. Finally, the dynamics of the contact line on the rods have been ignored as has any contact angle hysteresis. Since the surface of the rods is rough, the contact line may well be pinned (as appears to be the case from informal observations) and so this assumption is also reasonable.

Without the above assumptions, our simple analysis would founder. The naive model presented here, however, appears to encapsulate the essential physics of the problem since it has allowed us to understand the results of simple experiments qualitatively and, to a degree, quantitatively. Within our formulation, many interesting questions remain to be answered such as the role of self-interaction and the dynamics of a flexible hair interacting with a wall. Another possibility is the modelling of what might be termed 'Janus trains' consisting of alternate rods which attract/repel the wall (and are thus reminiscent of the Janus beads studied by Ondarçuhu *et al.* 1990). Experimentally this could be achieved in two ways: either by coating the sides of the rods differently so that one type is hydrophilic and the other hydrophobic; or rods of different density would cause different meniscus curvatures leading to analogous effects.

We are grateful to David Quéré for supplying the polymeric thread used to turn rods into trains. D. V. was supported by a summer studentship from the Heilbronn Fund of Trinity College. H. Y. K. was supported by a collaborative grant from the Royal Society and the Korea Science and Engineering Foundation. L. M. was supported by the Schlumberger Chair Fund and the US Office of Naval Research Young Investigator Program.

## REFERENCES

Bragg, L. & Nye, J. F. 1947 A dynamical model of a crystal structure. *Proc. R. Soc. Lond.* A **190**, 474–481.

Chan, D. Y. C., Henry, J. D. Jr. & White, L. R. 1981 The interaction of colloidal particles collected at a fluid interface. *J. Colloid Interface Sci.* **79**, 410–418.

Danov, K. D., Dimova, R. & Pouligny, B. 2000 Viscous drag of a solid sphere straddling a spherical or flat surface. *Phys. Fluids* **12**, 2711–2722.

Gifford, W. A. & Scriven, L. E. 1971 On the attraction of floating particles. *Chem. Engng Sci.* **26**, 287–297.

Happel, J. & Brenner, H. 1965 *Low Reynolds Number Hydrodynamics*. Kluwer.

Nicolson, M. M. 1949 The interaction between floating particles. *Proc. Camb. Phil. Soc.* **45**, 288–295.

Ondarçuhu, T., Fabre, P., Raphaël, E. & Veyssié, M. 1990 Specific properties of amphiphilic particles at fluid interfaces. *J. Phys. Paris* **51**, 1527–1536.

Paunov, V. N., Kralchevsky, P. A., Denkov, N. D. & Nagayama, K. 1993 Lateral capillary forces between floating submillimeter particles. *J. Colloid Interface Sci.* **157**, 100–112.

Rayleigh, Lord 1945 *The Theory of Sound*, Vol. 1, p. 102. Dover.

Ruhoff, P. T., Præstgaard, E. & Perram, J. W. 1996 Efficient algorithms for simulating complex mechanical systems using constraint dynamics. *Proc. R. Soc. Lond.* A **452**, 1139–1165.

Vincze, A., Demkó, L., Vörös, M., Zrínyi, M., Esmail, M. N. & Hórvölgyi, Z. 2002 Two-dimensional aggregation of rod-like particles: a model investigation. *J. Phys. Chem.* B **106**, 2404–2414.

Whitesides, G. M. & Grzybowski, B. 2002 Self-assembly at all scales. *Science* **295**, 2418–2421.